Nano Energy 58 (2019) 347–354

Contents lists available at ScienceDirect

Nano Energy

journal homepage: www.elsevier.com/locate/nanoen

Full paper

Alkali ions pre-intercalated layered vanadium oxide nanowires for stable magnesium ions storage

Han Tang, Fangyu Xiong, Yalong Jiang, Cunyuan Pei, Shuangshuang Tan, Wei Yang, Maosheng Li, Qinyou An*, Liqiang Mai*

State Key Laboratory of Advanced Technology for Materials Synthesis and Processing, International School of Materials Science and Engineering, Wuhan University of Technology, Wuhan 430070, China

ARTICLE INFO

Keywords:
Alkali ions pre-intercalated
Layered vanadium oxides
Nanowires
Magnesium ions storage

ABSTRACT

Owing to the high energy density, high security and low price, rechargeable magnesium batteries (RMBs) are promising candidate for the next generation of high-performance batteries. However, the development of cathode materials for RMBs is hindered by the intensive polarization of Mg^{2+}, which tends to destroy the stability of crystal structure and results in the degradation of batteries. Pre-intercalating the different alkali ions in crystal structure is an effective strategy to improve the layered structure stability and electrochemical performance of materials. Herein, the alkali ions (Li^+, Na^+, K^+) pre-intercalation is presented to improve the structure stability of layered vanadium oxide (A-V_3O_8) for Mg^{2+} storage. From the result, the cycling performance of cathode is promoted with the pre-intercalation radius increase. To explain the optimizing principle, we use density functional theory (DFT) calculation to simulate the interaction effect between pre-intercalated cation and layered structure. Among intercalation compounds A-V_3O_8 (A = Li, Na, K), the electrochemical performance of Na^+ pre-intercalated materials (NaV_3O_8) is better than the most of cathode materials for RMBs. Besides, the reaction mechanism of NaV_3O_8 is demonstrated. This work confirms that the pre-intercalation of appropriate alkali cation is an efficient strategy to improve the electrochemical performance of layered cathode materials for RMBs.

1. Introduction

Lithium-ion batteries (LIBs) have been researched intensively in electrochemical energy storage device and the relevant technological problems are solved gradually [1–6]. However, some problems such as safety issues, high prices, resource scarcity and insufficient energy density still hinder the further development of LIBs [7,8]. Rechargeable magnesium battery has been considered as a promising alternative to LIBs in recent years, due to the advantages of magnesium metal anode [9–11]. Compared with lithium, magnesium could avoid one-dimension dendrite because of its uniform deposition/dissolution property [12,13], which could avert the short circuit of battery. Moreover, when exposed to air, magnesium is safer and more convenient to handle due to the relatively stable chemical properties and oxide surface passivation [14,15]. Furthermore, magnesium is the fifth most abundant metallic element in the earth crust and more available (cost less than 1/24 of lithium) [10]. Magnesium also provides a high theoretical specific capacity of 2230 mA h g^{-1} and 3832 mA h cm^{-3} [16,17]. However, the development of RMBs is still sluggish and insufficient due to the dissatisfactory Mg^{2+} intercalated cathode materials [18]. The large charge-mass ratio of Mg^{2+} results in strong polarization effect and the sluggish diffusion rate when Mg^{2+} intercalate and migrate in the cathode materials [19]. For the above reasons, most commercial cathode materials for LIBs exhibit the poor electrochemical performance in RMBs [20]. Thus, developing the high performance cathode materials is one of the most urgent tasks in RMBs [18,21,22].

In 2000, Aurbach et al. found that the Chevrel phase Mo_6S_8 is an excellent cathode material for RMBs with excellent cycling performance (> 2000 cycles) [23]. Regrettably, Chevrel phase Mo_6S_8 only exhibit a low discharge voltage around 1.1 V (vs. Mg^{2+}/Mg) and the limited theoretical specific capacity of 128.8 mA h g^{-1}. Thus, the low energy density restricts the further development of Mo_6S_8. To improve the energy density, various vanadium oxides with large capacity and high working voltage were researched in RMBs. In vanadium oxides, multifarious chemical valences of vanadium elements and facile distortion of V-O bonds generate diverse vanadium oxides with extremely high capacity [24]. Therefore, vanadium oxides are the potential candidate cathode materials to the high energy density RMBs [25]. In 2013,

* Corresponding authors.
E-mail addresses: anqinyou86@whut.edu.cn (Q. An), mlq518@whut.edu.cn (L. Mai).

https://doi.org/10.1016/j.nanoen.2019.01.053
Received 13 December 2018; Received in revised form 11 January 2019; Accepted 15 January 2019
Available online 16 January 2019
2211-2855/

Gershinsky et al. reported V_2O_5 as cathode materials in RMBs, which delivered the high specific capacity of ~180 mA h g^{-1} in the first cycle and remained ~150 mA h g^{-1} after 35 cycles with the discharge plateau around 2.2 V. Except V_2O_5, layered vanadium bronzes have also attracted much attention of researchers, owing to the existence of interlayer ions which linked the layered structure and stabilized the crystal framework. Moreover, in V_3O_8 layer of vanadium bronzes, the special zigzag chains consisted by VO_5 trigonal bipyramids could provide more vacancies for guest ions intercalation [26]. The edge shared interconnection of VO_5 trigonal bipyramids are more flexible and could accommodate the higher levels of structural deformations when compared with normal VO_6 octahedrons [27]. Therefore, the vanadium oxides with V_3O_8 layer could insert more bivalent Mg^{2+}, possess higher specific capacity and exhibit better cycling stability. Besides, the vanadium oxide with V_3O_8 layer also possess large interlamellar spacing which further improve the space for guest ions storage and diffusion [27]. Novak et al. reported the vanadium bronzes applied in Mg^{2+} storage at first [28]. These vanadium bronzes exhibit the high initial discharge capacity about 170 mA h g^{-1}. However, the low coulombic efficiency and fast capacity decay in the first 15 cycles limited the further development of these vanadium bronzes. Moreover, the reaction mechanism of these vanadium bronzes in Mg^{2+} storage is still unclear. Although the different vanadium oxides exhibit high specific capacity, the cycling performance is still an intractable challenge.

Pre-intercalating the appropriate ions in cathode materials is an effective way to improve the structure stability and cyclability [29–32]. Herein, we presented the alkali ions pre-intercalation strategy to improve the structure stability of vanadium oxides during the Mg^{2+} intercalation/deintercalation process. Moreover, we also researched the different optimization effect of pre-intercalated alkali ions (Li^+, Na^+, K^+) to the electrochemical performance of materials (as V_3O_7 is not the layered structure, there is no comparability to the V_3O_7). The vanadium oxide with pre-intercalation of Na^+ (NaV_3O_8) in layered space possesses more stable crystal structure and exhibits the best magnesium ions storage performance. In addition, to ascertain the reaction mechanism, the structure evolution of NaV_3O_8 in Mg^{2+} storage process was investigated deeply by ex-situ X-ray diffraction (XRD) and X-ray photoelectron spectroscopy (XPS).

2. Experimental section

2.1. Material synthesis

LiV_3O_8 nanowires were synthesized from $H_2V_3O_8$ nanowires. $H_2V_3O_8$ nanowires were synthesized by hydrothermal method. Briefly, corresponding aniline and 1.2 mmol V_2O_5 sol were mixed under constant stirring for 1 h. Then, 0.04 g polyethylene glycol (PEG-4000) was added into solution. Finally, the above solution was transferred to Telfon-lined stainless steel autoclave, kept in 180 °C for 48 h. Dark green products could get after washed by deionized water and ethanol, respectively. To LiV_3O_8, $H_2V_3O_8$ nanowires was mixed in alcohol and $LiOH{\cdot}H_2O$ (V/Li = 3:1.05) were added. After stirred for 5 h, the mixture was heated at 80 °C and then annealed in 450 °C in air to obtain LiV_3O_8 products. NaV_3O_8 (KV_3O_8) was synthesized from V_2O_5 powder and NaOH (KOH) by hydrothermal method. Briefly, 1.8 g V_2O_5 (0.9 g for KV_3O_8) powder and 0.4 g NaOH (0.2 g KOH) were mixed in deionized water (40 ml) and stirred for 30 min. Then, the above solution was transferred to Telfon-lined stainless steel autoclave, kept in 180 °C for 48 h. Finally, these products were treated at 500 °C (400 °C for KV_3O_8) for 3 h in air and washed by deionized water and ethanol, respectively.

2.2. Material characterizations

To investigate the crystallographic information, the XRD patterns were recorded by using a Bruker D8 Advance X-ray diffractometer with a non-monochromated Cu Kα X-ray source. Scanning electron microscopy (SEM) images were collected with a Jeol JSM-7100F field emission scanning electron microscope at an acceleration voltage of 20 kV. Transmission electron microscopy (TEM) and high resolution transmission electron microscopy (HRTEM) images were carried out by using the Jeol JEM-2100F scanning transmission electron microscope/energy dispersive X-ray spectroscopy (EDX) microscope and titan G2 60-300 with image corrector. Inductively Coupled Plasma Optical Emission Spectroscopy analysis (ICP-OES) is JY/T015-1996. Atomic Absorption Spectroscopy (AAS) is CONTRAA-700.

2.3. Electrochemical measurements

The synthetic A-V_3O_8 (A = Li, Na, K) products, acetylene black, and polytetrafluoroethylene (PTFE) were mixed in a weight ratio of 6:3:1 and then grinded in agate mortar sufficiently about 30 min. Next they were put into steel mash with an area about 0.5 cm^2 and a loading of ~1.5 mg cm^{-2}. Finally, the disks of cathode material was dried in the vacuum drying oven about 12 h. To three-electrode cell, activated carbon (AC) clothes are both used as counter and reference electrode. The potential of AC cloth was measured to be 0.12 V vs. ferrocene/ferrocenium, i.e. 2.4 V vs. Mg^{2+}/Mg [33]. The working electrodes were operated within −1 to 0.7 V vs. AC, equivalent to 1.4–3.1 V vs. Mg^{2+}/Mg. To coin cell, the glass microfibre membrane was chosen as the separator. Mg metal was polished with sandpaper and pushed into disks as anode before use. These parts were assembled orderly by CR2016 coin cells in glove box. Galvanostatic charge/discharge cycling, cyclic voltammetry were measured using a potentiostat (Bio-Logic VMP-3). All the materials were tested in the inert atmosphere glove box (argon, both moisture and oxygen concentrations were under 0.1 ppm).

3. Results and discussion

To compare the structure difference of A-V_3O_8 (A = Li, Na, K), powder XRD pattern of them are exhibited in Fig. 1a-b. The diffraction peaks of A-V_3O_8 (A = Li, Na, K) are well indexed to JCPDS No.01-072-1193, JCPDS No.00-028-1171, JCPDS No.00-022-1247, respectively, indicating a pure phase of these vanadium oxides. The interlayer space of Li, Na, K, -V_3O_8 enlarge regularly with radius increasing of pre-intercalations (LiV_3O_8 = 6.32 Å, NaV_3O_8 = 6.85 Å, KV_3O_8 = 7.48 Å), indicating the layered structure is affected significantly by the size of the pre-intercalated alkali cations. Fig. 1c-e reveals the crystal structure of A-V_3O_8 (A = Li, Na, K). The layered structure of LiV_3O_8 and NaV_3O_8 are both composed of VO_6 octahedrons and VO_5 trigonal bipyramids which share edges and corners by oxygen atoms (Fig. 1c-d). Specifically, four VO_6 octahedrons as the structure unit form double chains of $(V_4O_{20})_n$ and two VO_5 trigonal bipyramids as the structure unit form zigzag chains of $(V_2O_8)_n$, respectively. Then, the $(V_4O_{20})_n$ and $(V_2O_8)_n$ chains constitute the V_3O_8 layer of LiV_3O_8 and NaV_3O_8 by edge-sharing oxygen atoms. The layer of KV_3O_8 also consists of V_2O_8 units and VO_6 octahedrons, sharing edges and corners by oxygen atoms [34]. But the connection type and sequence of V-O polyhedrons in KV_3O_8 are different with that of LiV_3O_8 and NaV_3O_8. Specifically, two VO_5 square pyramids are connected by one VO_6 octahedron and form $(V_3O_{12})_n$ chains stacked along *c* axis. Then, another reversed $(V_3O_{12})_n$ chains link the above $(V_3O_{12})_n$ chains and form V_3O_8 layers of KV_3O_8 along *b* axis (Fig. 1e) [26]. Therefore, the layered structure of KV_3O_8 is different with that of the LiV_3O_8 and NaV_3O_8, which might result from the large atomic radius of K atom. On the other hand, the morphology of A-V_3O_8 (A = Li, Na, K) were explored by scanning electron microscope (SEM) and transmission electron microscope (TEM) (Fig. S1). Element mapping pattern (Fig. S2) indicated that the elements of V, O are uniformly distributed within the A-V_3O_8 (A = Li, Na, K) and Na, K are distributed within NaV_3O_8 and KV_3O_8, respectively.

To explore the influence of pre-intercalation and electrochemical insertion performance of Mg^{2+} in layered A-V_3O_8 (A = Li, Na, K). These layered vanadium oxides were assembled as cathode materials in

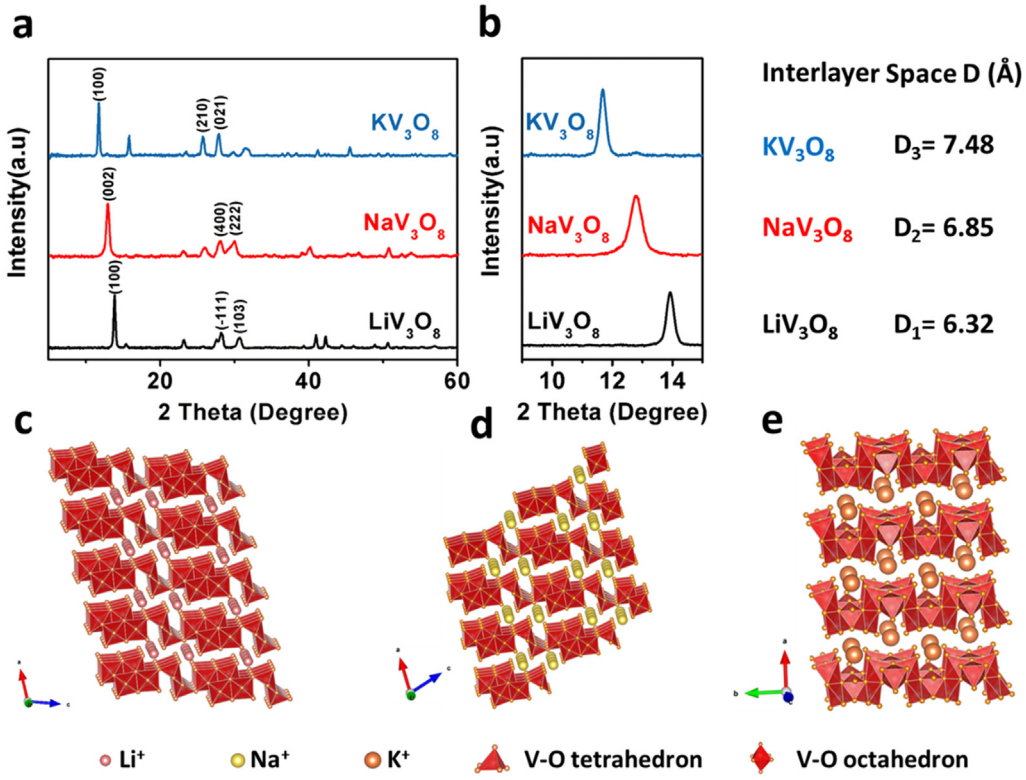

Fig. 1. (a) XRD pattern, (b) interlayer space, and (c-e) illustration of the crystal structure of A-V_3O_8 (A= Li, Na, K).

three-electrode cell. 0.5 M $Mg(ClO_4)_2$ in acetonitrile (CH_3CN) is used as electrolyte and activated carbon clothes (AC) are chosen both as counter and quasi-reference electrode. The calibrated potential of AC electrode is 2.4 V (vs. Mg^{2+}/Mg)[33]. First, cyclic voltammetry (CV) curves were measured at 0.1 mV s^{-1} (Fig. 2a). The cathodic and anodic peaks are associated with Mg^{2+} insertion and extraction in the cathode materials, respectively. In the CV curves of these materials, both cathodic and anodic peaks decrease regularly with the pre-intercalated alkali cations radius increase (LiV_3O_8 > NaV_3O_8 > KV_3O_8). This phenomenon might result from the different interaction effect between Mg^{2+} and pre-intercalated alkali cations, which we will discuss in the calculation part. Charge and discharge curves of A-V_3O_8 (A = Li, Na, K) at 100 mA h g^{-1} are exhibited in Fig. 2b. A-V_3O_8 (A = Li, Na) possess high specific capacity of 252.2, 204.16 mA h g^{-1}, respectively. Unfortunately, KV_3O_8 obtains low specific capacity of only 37.56 mA h g^{-1}. The cycling performance of A-V_3O_8 (A = Li, Na, K) at 100 mA g^{-1} are demonstrated at Fig. 2c. After 30 cycles, A-V_3O_8 (A = Li, Na, K) still maintain specific capacity of 106.4, 174.99 and 33.29 mA h g^{-1}, respectively. Their capacity retention ratios are 42.2%, 85.78% and 88.6%, respectively. From the result, the cycling performance is KV_3O_8 > NaV_3O_8 > LiV_3O_8, illustrating that the larger pre-intercalated alkali cations can prevent the structure destruction to greater extent. In order to further explore the electrochemical kinetics of A-V_3O_8 (A = Li, Na, K), the electrochemical impedance spectroscopy (EIS) was measured. The Nyquist plots of A-V_3O_8 (A = Li, Na, K) reveal a depressed semicircle in the high-frequency region and a straight line in the low-frequency region (Fig. S3). The radius of the depressed semicircle is related to the charge transfer impedance (R_{ct}). The straight line is associated with the Warburg impedance (W). In the comparison of the materials, the R_{ct} of the A-V_3O_8 (A = Li, Na) is smaller than that of KV_3O_8, illustrating that Li^+, Na^+ in crystal structure might improve the electronic conduction of vanadium materials. On the other hand, the Warburg impedance is mainly connected to the diffusion of Mg^{2+} in cathodes materials in which NaV_3O_8 > LiV_3O_8 and this result might account for the excellent electrochemical performance of NaV_3O_8.

To investigate the influence of pre-intercalated alkali cations on electrochemical insertion/extraction behavior of Mg^{2+}. The Mg^{2+} intercalation process in A-V_3O_8 (A = Li, Na, K) is simulated based on DFT. From the calculate result (Fig. 2d, Fig. S4 and Table S1), the intercalation energies of Mg^{2+} in LiV_3O_8 (−5.63 eV), NaV_3O_8 (−5.4 eV) KV_3O_8 (−4.74 eV) rises with the increase of pre-intercalated ion radius, which could explain the regular increase of the cathodic peaks in CV curves of these materials. Therefore, this result indicates that pre-intercalating alkali cations can adjust the discharge voltage of vanadium oxides in RMBs.

To further explain the complicated mechanism about the different optimization effect in cycling stability after different alkali cations pre-intercalation, we investigate the structure stability of A-V_3O_8 (A = Li, Na, K) based on the diffusion process (via energy barrier, $E_{barrier}$) of pre-intercalated A ions in V_3O_8 layers without considering Mg^{2+} intercalation (Fig. 2e). Fig. 2g-i exhibit the most probable diffusion path of pre-intercalated alkali cations in A-V_3O_8 (A = Li, Na, K). The diffusion barrier comparison of pre-intercalation is that K (1.91 eV) > Na (0.64 eV) > Li (0.33 eV). From the result, the migration of larger pre-intercalated cations in the interlayer space will result in the greater distortion of V-O single bond, leading to the larger diffusion barrier of pre-intercalated cations [24]. Therefore, the diffusion and de-intercalation of large pre-intercalated cations will be restricted, and the pre-intercalated ions can act as stable “pillar” in the interlayer space. The “pillar” will prevent the relative slippage between the two adjacent V-O layers and support two layers which stabilize the V-O layered structure and avoid the structure collapse vertically. However, if the cation with oversize-radius (e.g. K ion) pre-intercalated into the interlayer space of vanadium-based materials, the guest ions will difficult to intercalate into the materials, resulting in the low specific capacity. On the other hand, the oversize-radius pre-intercalation will also change the layered structure of vanadium oxide largely (the layered structure of KV_3O_8 is different with the A-V_3O_8 (A = Li, Na)), which may also restrains the intercalation of Mg^{2+} and results in the low specific capacity. The V_3O_8 layers will selectively combine the intercalated cations and adjust the

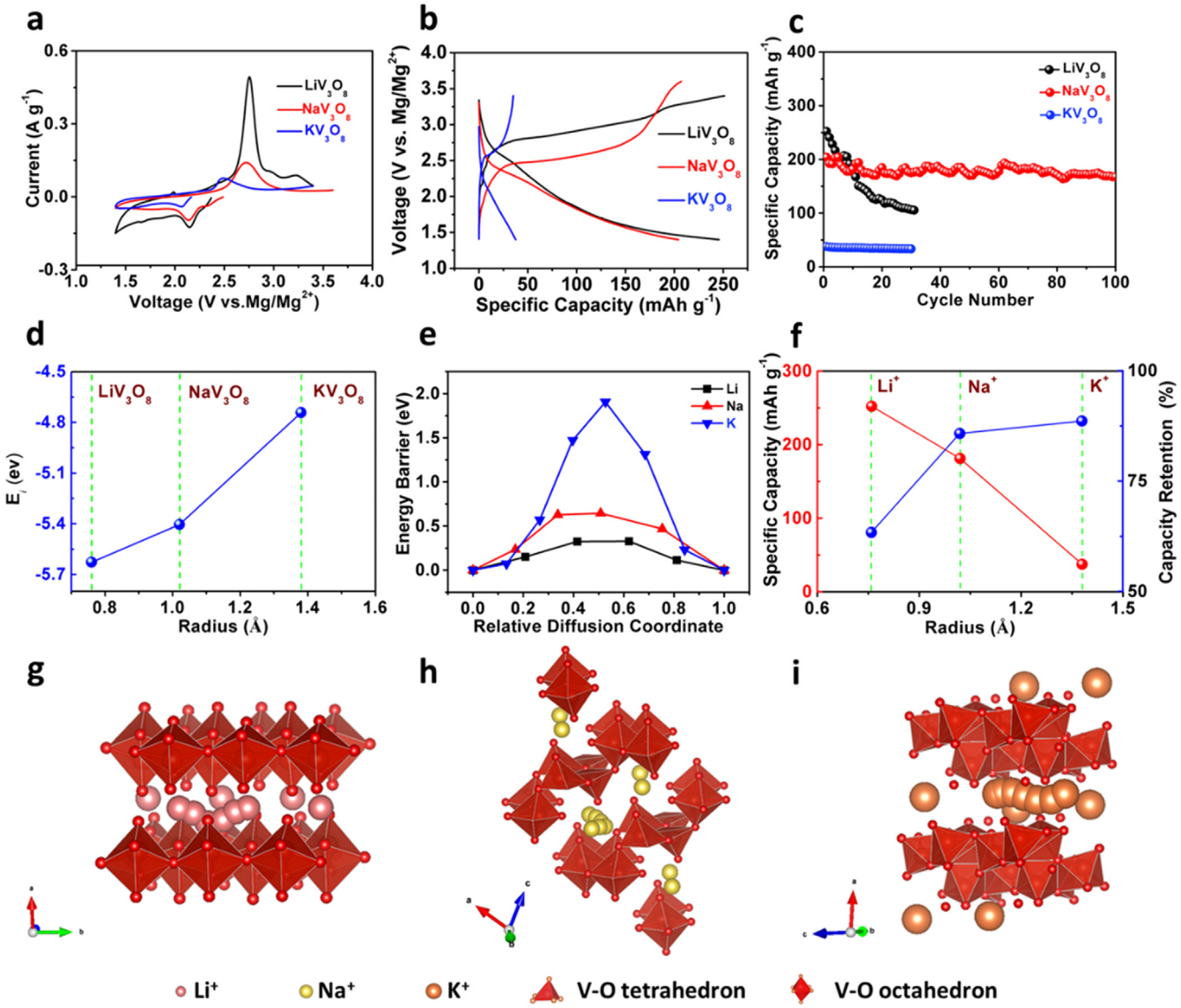

Fig. 2. Electrochemical performance of A-V_3O_8 (A = Li, Na, K). (a) CV curves of A-V_3O_8 (A = Li, Na, K) at scan rate of 0.1 mV s^{-1}. (b) Charge and discharge curves of A-V_3O_8 (A = Li, Na, K) at current density of 100 mA g^{-1}. (c) Cycling performance of A-V_3O_8 (A = Li, Na, K) at the current density of 100 mA g^{-1}. (d) Mg^{2+} intercalation energies (E*i*) in A-V_3O_8 (A = Li, Na, K). (e) Energy barrier for Li, Na, K atom along the diffusion paths in V-O layers. (f) Specific capacity of A-V_3O_8 (A = Li, Na, K) at 100 mA g^{-1} and the capacity retention of A-V_3O_8 (A = Li, Na, K) after 30 cycles. (g-i) The diffusion path of pre-intercalated cations (Li, Na, K) in crystal structure of vanadium oxides.

layered structure according to the intercalated ionic size. Therefore, the interaction effect between layered structure and intercalated cations decided by the category and property of intercalated cations [24]. From the above, these results are different with our previous work about pre-intercalation with V_2O_5 [24], which might result from the different layered structure of V_2O_5 and V_3O_8.

According to the comprehensive consideration of both specific capacity and cycling stability of three samples (Fig. 2f), the electrochemical performance of NaV_3O_8 is the best one. Thus, the NaV_3O_8 was selected as representative to further investigate in detail. The rate performance of NaV_3O_8 is shown in Fig. 3a and the charge/discharge curves are shown in Fig. S5. The high capacity of 260 mA h g^{-1} is obtained at the current density of 50 mA g^{-1}. This result declares that the NaV_3O_8 is a potential candidate for high capacity cathode materials in RMBs. At higher current density of 100, 200, 500 and 1000 mA g^{-1}, the specific capacities of 184, 123.9, 86.6, 62.4 mA h g^{-1} are still obtained, respectively. In long-term cycling performance test, NaV_3O_8 could maintain more than 60 mA h g^{-1} (88.3% of initial specific capacity) after 100 cycles at the high current density of 500 mA g^{-1} (Fig. S6). We also tested the electrochemical performance of NaV_3O_8 in $(PhMgCl)_2$/$AlCl_3$/THF (APC) and $MgCl_2$/$AlCl_3$/DME (MACC) electrolyte, which is active for reversible Mg platting/stripping (Fig. S7 a, c). However, NaV_3O_8 only exhibits low specific capacity in these electrolytes (Fig. S7 b, d). This phenomenon might result from the compatibility problem, which often appeared in various vanadium oxides [35]. In order to confirm the insertion/extraction of Mg^{2+}, High Angle Annular Dark Field (HAADF) images and EDS elemental mappings of NaV_3O_8 at initial, discharge and charge state were measured (Fig. 3b-c, Fig. S8). In different state, Na, V, O elements are distributed within the NaV_3O_8 nanowires uniformly. In initial state, there is no Mg element existed in the materials (Fig. S8a). After discharge process, abundant Mg element is discovered in the NaV_3O_8 nanowires (Fig. 3c), indicating that the Mg^{2+} in electrolyte have intercalated into the NaV_3O_8 nanowires. In charge state, only a small quantity of Mg element could be found in the NaV_3O_8 nanowires (Fig. S8b), indicating the extraction of Mg^{2+}. The mapping result provides visual proof about the Mg^{2+} intercalation/

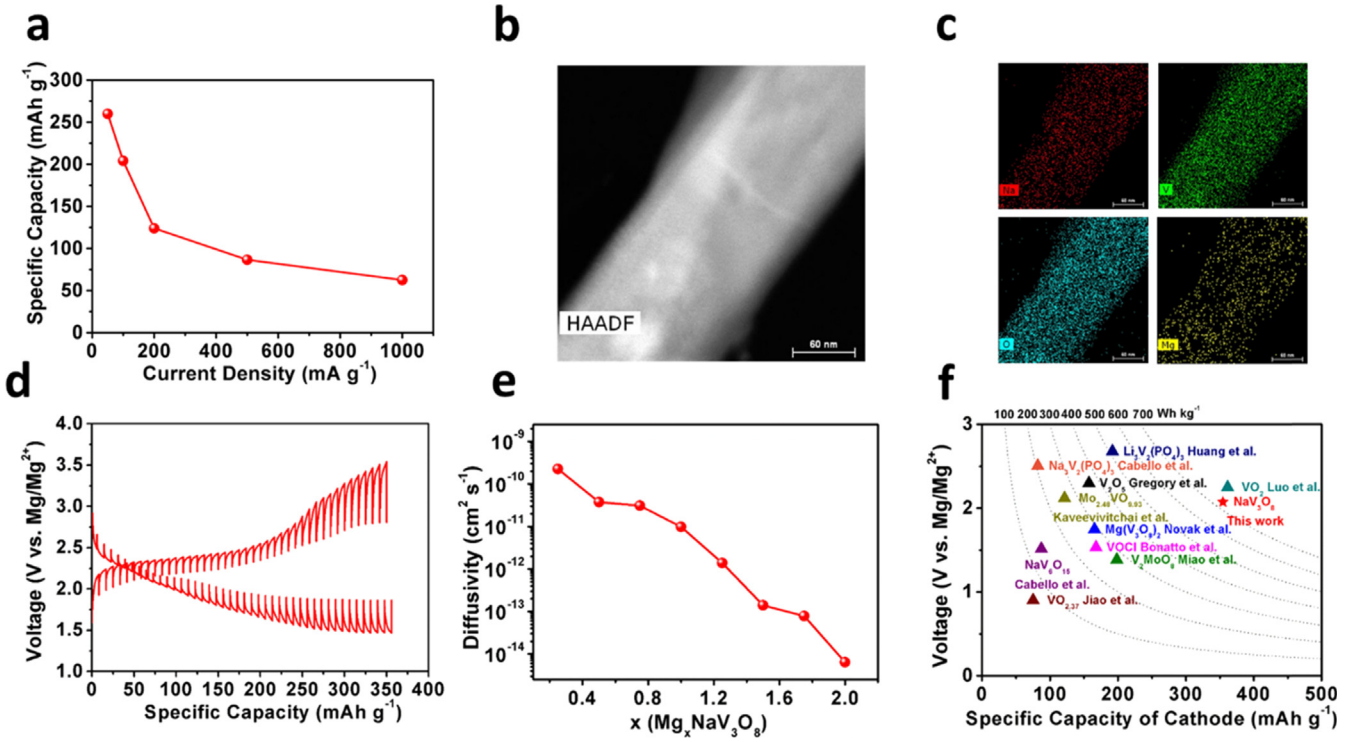

Fig. 3. (a) Rate performance of NaV_3O_8. (b) HAADF image and (c) EDS elemental mappings of NaV_3O_8 at discharge state. (d) The galvanostatic intermittent titration technique (GITT) curves of NaV_3O_8 at 50 mA g^{-1}. (e) Mg^{2+} diffusivity at different discharge state. (f) Specific energy density comparison of vanadium-based cathode materials in magnesium batteries.

extraction process in NaV_3O_8 nanowires. The ICP result also certifies the intercalation/extraction process of Mg^{2+} (Table S2). To further study the structure change of NaV_3O_8 cathode in cycling process, we also measured the Na^+ concentration in the electrolyte before and after cycling and we found that a small amount of Na^+ might be extracted from the NaV_3O_8 (Table S3). To investigate the maximum capacity of NaV_3O_8 and diffusion coefficient of Mg^{2+}, the galvanostatic intermittent titration technique (GITT) curve was measured. In Fig. 3d, NaV_3O_8 could obtain the high capacity of 350 mA h g^{-1}, corresponding to 2 mol Mg^{2+} intercalation for per mole of NaV_3O_8. This capacity is very high among the reported cathode materials in RMBs [19,35–42]. Furthermore, the Mg^{2+} diffusivity (D^{GITT}) can be calculated from the slight potential response (Fig. S9) with the formula (Scheme 1 in Supporting information). The Mg^{2+} diffusivity decreases from 2.25×10^{-10} to 6.45×10^{-15} with the intercalation capacity increasing of Mg^{2+} (Fig. 3e). This phenomenon might result from the intense electrostatic repulsion when more Mg^{2+} occupied the active sites. On the other hand, the discharge capacity and operation voltage of various vanadium-based cathode materials in RMBs have been summarized to compare the energy density (Fig. 3f) [19,28,36–41]. The energy density of NaV_3O_8 in this work could achieve 700 Wh kg^{-1} (based on the weight of cathode material), much higher than most other vanadium-based materials in RMBs. Although the energy density of VO_2 reported by Lou et al. is higher than NaV_3O_8, the cycling stability of NaV_3O_8 is better [40]. Considering from multiple factor synthetically, NaV_3O_8 is a promising cathode material in RMBs.

Besides, exploring the crystal structure evolution and reaction mechanism during the cycling process is important for further promoting the electrochemical performance of NaV_3O_8. Thus, the ex-situ XRD was performed to investigate the crystal structure change of NaV_3O_8 at different charge and discharge stages. In Fig. 4a, there is no peak generate or disappear in the cycling process. Fig. 4b is the enlarge view of ex-situ XRD result of NaV_3O_8 between 12° and 20° (the peak in 18° is contributed by the polytetrafluoroethylene (PTFE) which acts as binder in cathode slice) [43]. The main peak (002) of NaV_3O_8 in 12.66° shifts obviously, which links to the change of layer spacing. When NaV_3O_8 was discharged to 1.8 V, the peak (002) shifts to higher angle, indicating the contract of layer distance. This phenomenon might come from the coordination between intercalated Mg^{2+} and oxygen element. This abnormal phenomenon often takes place in layered vanadium oxide materials [44,45]. After discharge to 1.4 V (III), the (002) peak shift to lower degree, which indicated that more Mg^{2+} intercalated into the layered structure and the interlayer space enlarged. Plenty of Mg^{2+} inserting into the layered structure will result in the powerful electrostatic repulsion effect and the V-O layered structure will be expanded due to the repulsive interaction from Mg^{2+}. In the charging process (III→IV→V), the peak (002) shift to higher degree, indicating the contract of interlayer space. The partial Mg^{2+} in layered structure extracting from the NaV_3O_8 alleviates the electrostatic repulsion effect and the layer spacing reduces. After charge to 3.6 V (VI), the (002) peak shifts to lower degree, corresponding with the expansion of layer spacing. A large amount of Mg^{2+} extracting from the layer spacing will reduce the coordination action between Mg^{2+} and oxide atoms, leading to the increase of interlayer space. However, the (002) peak in VI stage did not reverse to initial stage, indicating that the distance of V-O layers in charged stage is still smaller than that of initial stage. Some Mg^{2+} might remained in the layered spacing and provide partial coordination reaction with oxygen, leading to the contract of V-O layers. These series of changes are illustrated in Fig. 4d. From the above, the ex-situ XRD result illustrates that it is the single-phase reaction in NaV_3O_8 during the Mg^{2+} intercalation/deintercalation. To explore the valence variation of vanadium elements, ex-situ XPS tests of NaV_3O_8 in initial, discharged and charged stages were performed (Fig. 4c). For pristine NaV_3O_8, the *2p* core level spectrum of vanadium displays two asymmetrical peaks related to the V2$p_{3/2}$ and V 2$p_{1/2}$ orbital. The V2$p_{3/2}$ peak could be divided into a main peak and a weak peak, corresponding to V^{5+} (517.3 eV) and V^{4+} (516.3 eV), respectively, confirming the slight existence of V^{4+}. After discharge to 1.4 V, the peak of V^{5+} weaken and the peak of V^{4+} strengthen, indicating that a part of V^{5+} are reduced to V^{4+} when Mg^{2+} intercalate into the NaV_3O_8. In charge

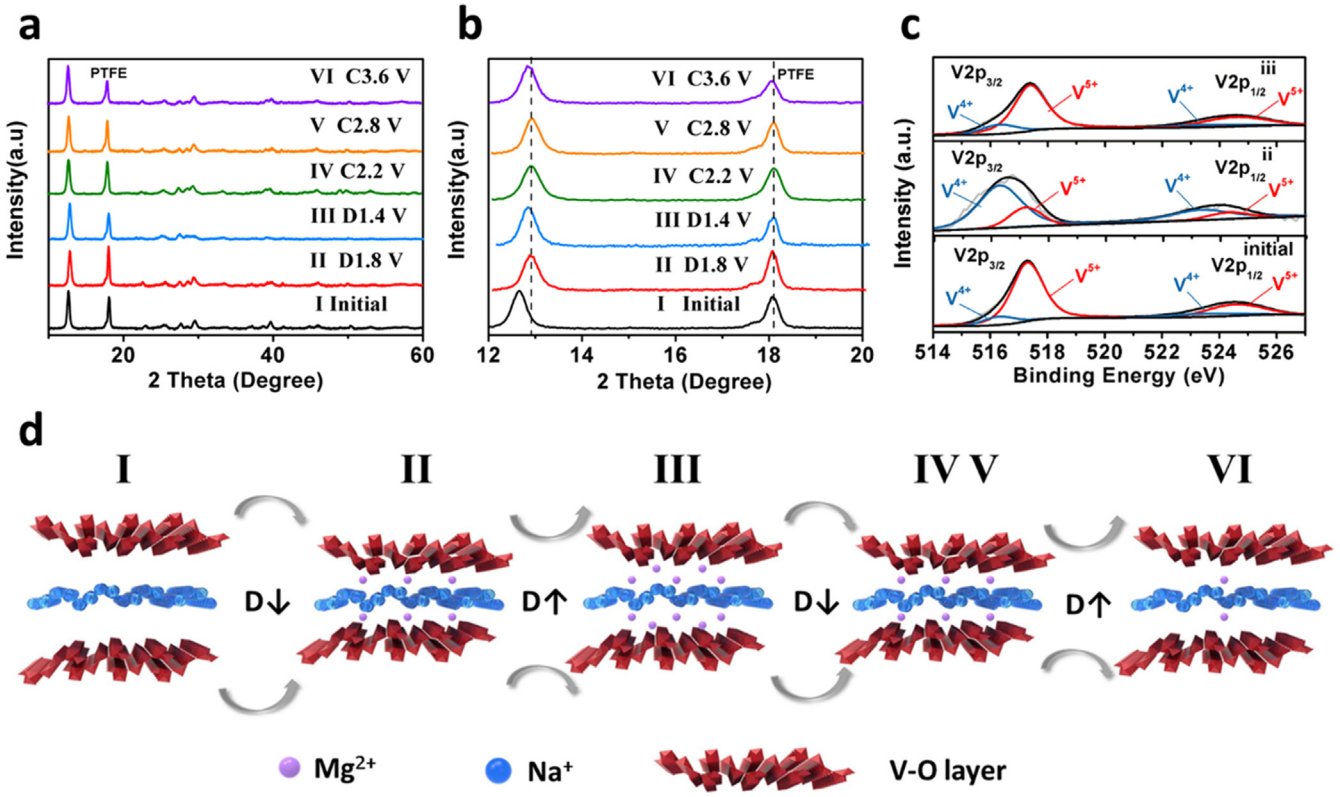

Fig. 4. (a-b) Ex-situ XRD patterns, (c) XPS spectra of NaV_3O_8 in different status in the first cycle. (d) Interlayer space change of NaV_3O_8 in different charge and discharge stage.

state, the peak of V^{5+} and V^{4+} return to the original condition basically, illustrating the good reversibility of NaV_3O_8 in Mg^{2+} insertion/extraction process. From above result, NaV_3O_8 could maintain the structure stability when Mg^{2+} insert/extract from the layered spacing and is a potential cathode material for RMBs.

4. Conclusions

We have systematically explored the alkali cations (Li^+, Na^+, K^+) pre-intercalated vanadium oxides as optimized cathode materials for magnesium batteries, basing on structure analysis, electrochemical tests and DFT calculation. The pre-intercalation with Na^+ yields a more stable interlayer structure, which allows Mg^{2+} to diffuse freely and prevent the destructive collapse of layers. It is indicated that appropriate pre-intercalated ions in layered structure can optimize Mg^{2+} intercalation capacity and cycling performance in magnesium batteries. This phenomenon is attributed to the stabilizing effect between layered structure and intercalated alkali ions. The intercalated ions will act as "pillars" to stabilize the layered space and buffer space to accommodate the expansion/contraction of layered structure during charge and discharge process. This kind of optimizing strategy provides an effective and available way to regulate diffusion channel of vanadium oxides. On the other hand, the structure evolution and the single-phase reaction mechanism of NaV_3O_8 in magnesium ions storage have been revealed for the first time, which is instructive and meaningful to the further optimization in the Mg^{2+} storage of layered vanadium-based materials.

Acknowledgements

This work was supported by the National Natural Science Fund for Distinguished Young Scholars (51425204), the National Key R&D Program of China (2016YFA0202601 and 2016YFA0202603), the National Natural Science Foundation of China (51602239, 51832004), the International Science & Technology Cooperation Program of China (2013DFA50840), the Fundamental Research Funds for the Central Universities (WUT: 2017III009).

Appendix A. Supporting information

Supplementary data associated with this article can be found in the online version at doi:10.1016/j.nanoen.2019.01.053.

References

[1] S. Chu, A. Majumdar, Nature 488 (2012) 294–303.
[2] J. Deng, H. Ji, C. Yan, J. Zhang, W. Si, S. Baunack, S. Oswald, Y. Mei, O.G. Schmidt, Angew. Chem. 52 (2013) 2382–2386.
[3] B. Dunn, H. Kamath, J.M. Tarascon, Science 334 (2011) 928–935.
[4] L. Mai, X. Tian, X. Xu, L. Chang, L. Xu, Chem. Rev. 114 (2014) 11828–11862.
[5] K. Xu, Chem. Rev. 114 (2014) 11503–11618.
[6] C. Yan, W. Xi, W. Si, J. Deng, O.G. Schmidt, Adv. Mater. 25 (2013) 539–544.
[7] M. Armand, J.M. Tarascon, Nature 451 (2008) 652–657.
[8] B. Dunn, J.M. Tarascon, Science 334 (2011) 928–935.
[9] Y.K. Sun, Z. Chen, H.J. Noh, D.J. Lee, H.G. Jung, Y. Ren, S. Wang, C.S. Yoon, S.T. Myung, K. Amine, Nat. Mater. 11 (2012) 942–947.
[10] J. Muldoon, C.B. Bucur, A.G. Oliver, T. Sugimoto, M. Matsui, H.S. Kim, G.D. Allred, J. Zajicek, Y. Kotani, Energ. Environ. Sci. 5 (2012) 5941–5950.
[11] P. Canepa, G.S. Gautam, D.C. Hannah, R. Malik, L. Miao, K.G. Gallagher, K.A. Persson, G. Ceder, Chem. Rev. 117 (2017) 4287–4341.
[12] D. Aurbach, Y. Cohen, M. Moshkovich, Electrochem. Solid State Lett. 4 (2001) A113–A116.
[13] M. Matsui, J. Power Sources 196 (2011) 7048–7055.
[14] Y. Cheng, T. Liu, Y. Shao, M. Engelhard, J. Liu, G. Li, J. Mater. Chem. A 2 (2014) 2473–2477.
[15] H.D. Yoo, I. Shterenberg, Y. Gofer, G. Gershinsky, N. Pour, D. Aurbach, Energ. Environ. Sci. 6 (2013) 2265–2279.
[16] K. Itaoka, I.T. Kim, K. Yamabuki, N. Yoshimoto, H. Tsutsumi, J. Power Sources 297 (2015) 323–328.
[17] Y. Li, Q. An, Y. Cheng, Y. Liang, Y. Ren, C.J. Sun, H. Dong, Z. Tang, G. Li, Y. Yao, Nano Energy 34 (2017) 188–194.
[18] E. Levi, Y. Gofer, D. Aurbach, Chem. Mater. 22 (2010) 860–868.
[19] W. Kaveevivitchai, A.J. Jacobson, Chem. Mater. 28 (2016) 4593–4601.
[20] M. Mao, T. Gao, S. Hou, C. Wang, Chem. Soc. Rev. 47 (2018) 8804–8841.

[21] R.C. Massé, E. Uchaker, G. Cao, Sci. China Mater. 58 (2015) 715–766.
[22] F. Xiong, Y. Fan, S. Tan, L. Zhou, Y. Xu, C. Pei, Q. An, L. Mai, Nano Energy 47 (2018) 210–216.
[23] D. Aurbach, Z. Lu, A. Schechter, Y. Gofer, H. Gizbar, R. Turgeman, Y. Cohen, M. Moshkovich, E. Levi, Nature 407 (2000) 724–727.
[24] Y. Zhao, C. Han, J. Yang, J. Su, X. Xu, S. Li, L. Xu, R. Fang, H. Jiang, X. Zou, Nano Lett. 15 (2015) 2180–2185.
[25] Q. An, Y. Li, H.D. Yoo, S. Chen, Q. Ru, L. Mai, Y. Yao, Nano Energy 18 (2015) 265–272.
[26] S. Krachodnok, K.J. Haller, I.D. Willaims, Eng. J. 16 (2012) 19–28.
[27] Q. An, J. Sheng, X. Xu, Q. Wei, Y. Zhu, C. Han, C. Niu, L. Mai, New. J. Chem. 38 (2013) 2075–2080.
[28] P. Novak, W. Scheifele, F. Joho, O. Haas, J. Electrochem. Soc. 26 (1995) 2544–2550.
[29] E. Pomerantseva, Y. Gogotsi, Nat. Energy 2 (2017) 17089–17095.
[30] L. Yanliang, Y. Hyun Deog, L. Yifei, S. Jing, H.A. Calderon, L.C. Grabow, Y. Yan, Nano Lett. 15 (2015) 2194–2202.
[31] H.D. Yoo, Y. Liang, H. Dong, J. Lin, H. Wang, Y. Liu, L. Ma, T. Wu, Y. Li, Q. Ru, Nat. Commun. 8 (2017) 339–349.
[32] L. Zhou, Q. Liu, Z. Zhang, K. Zhang, F. Xiong, S. Tan, Q. An, Y.M. Kang, Z. Zhou, L. Mai, Adv. Mater. 30 (2018) 1801984.
[33] G. Gershinsky, H.D. Yoo, Y. Gofer, D. Aurbach, Langmuir 29 (2013) 10964–10972.
[34] Y. Oka, T. Yao, N. Yamamoto, Mater. Res. Bull. 32 (1997) 1201–1209.
[35] H. Tang, Z. Peng, L. Wu, F. Xiong, C. Pei, Q. An, L. Mai, Electrochem. Energy Rev. 1 (2018) 169–199.
[36] M. Cabello, R. Alcántara, F. Nacimiento, P. Lavela, M.J. Aragón, J.L. Tirado, Electrochim. Acta 246 (2017) 908–913.
[37] M. Cabello, F. Nacimiento, R. Alcántara, P. Lavela, G. Ortiz, J.L. Tirado, J. Electrochem. Soc. 163 (2016) A2781–A2790.
[38] Z.D. Huang, T. Masese, Y. Orikasa, T. Mori, K. Yamamoto, RSC Adv. 5 (2015) 8598–8603.
[39] L. Jiao, H. Yuan, Y. Si, Y. Wang, J. Cao, X. Gao, M. Zhao, X. Zhou, Y. Wang, J. Power Sources 156 (2006) 673–676.
[40] T. Luo, Y. Liu, H. Su, R. Xiao, L. Huang, Q. Xiang, Y. Zhou, C. Chen, Electrochim. Acta 260 (2017) 805–815.
[41] X. Miao, Z. Chen, N. Wang, Y. Nuli, J. Wang, J. Yang, S.I. Hirano, Nano Energy 34 (2017) 26–35.
[42] C.B. Minella, P. Gao, Z. Zhao-Karger, X. Mu, T. Diemant, M. Pfeifer, V.S.K. Chakravadhanula, R.J. Behm, M. Fichtner, ChemElectroChem 4 (2017) 738–745.
[43] P. He, M. Yan, G. Zhang, R. Sun, L. Chen, Q. An, L. Mai, Adv. Energy Mater. 7 (2017) 1601920–1601925.
[44] H. Tang, N. Xu, C. Pei, F. Xiong, S. Tan, W. Luo, Q. An, L. Mai, ACS Appl. Mater. Interfaces 9 (2017) 28667–28673.
[45] D. Wang, Q. Wei, J. Sheng, P. Hu, M. Yan, R. Sun, X. Xu, Q. An, L. Mai, Phys. Chem. Chem. Phys. 18 (2016) 12074–12079.

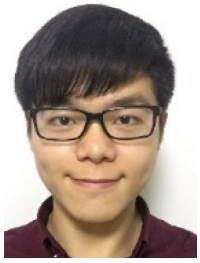

Han Tang received his B.S. degree in Department of Materials Science and Engineering from Hubei University of Technology in 2016. He is currently working toward the Ph.D. degree at Wuhan University of Technology. His current research involves the nanomaterials achieving high energy density and power density for rechargeable multivalent batteries.

Fangyu Xiong received his B.S. degree in Material Physics from Wuhan University of Technology in 2016. He is currently working toward the Ph.D. degree and his current research interests focuses on electrode materials for emerging energy storage devices.

Yalong Jiang received his B.S. degree in College of Material and Metallurgy from Wuhan University of Science and Technology in 2015. He is currently working toward the Ph.D. degree and focuses on energy storage materials and devices.

Cunyuan Pei received his B.S. degree in Department of Materials Science and Engineering from Hebei University of Architecture in 2014. He is currently working toward the Ph.D. degree and focuses on nanomaterials and electrolytes for magnesium ion battery.

Shuangshuang Tan received his B.S. degree in Material Science and Engineering from Wuhan University of Technology in 2016. He is currently working toward the Ph.D. degree and his current research focuses on the energy storage materials and devices.

Wei Yang received his Master's degree in Materials Engineering from Wuhan University of Technology in 2017. He is currently working toward the Ph.D. degree at Wuhan University of Technology. His research interests focus on developing functional materials for micro energy storage devices.

Maosheng Li received his B.S. degree from the College of Materials Science and Engineering, Beijing University of Chemical Technology. He is currently working toward M.S. degree at Wuhan University of Technology. His research focuses on the cathode material of multivalent metal batteries.

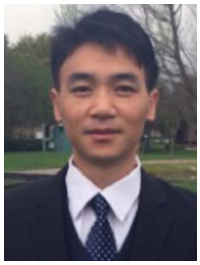

Qinyou An is Associate Professor of Materials Science and Engineering at Wuhan University of Technology (WUT). He received his Ph.D. degree from WUT in 2014. He carried out his postdoctoral research in the laboratory of Prof. Yan Yao at the University of Houston in 2014–2015. Currently, his research interest includes energy storage materials and devices.

Liqiang Mai is Chang Jiang Scholar Professor and Chair Professor of Materials Science and Engineering at Wuhan University of Technology (WUT). He received his Ph.D. degree from WUT in 2004. He carried out his postdoctoral research in Prof. Zhonglin Wang's group at Georgia Institute of Technology in 2006–2007. He worked as advanced research scholar in the laboratory of Prof. Charles M. Lieber at Harvard University in 2008–2011 and the laboratory of Prof. Peidong Yang at University of California, Berkeley in 2017. His current research interests focus on new nanomaterials for electrochemical energy storage and micro/nano energy devices.